Arabian Journal of Chemistry (2023) **16**, 104846

King Saud University

Arabian Journal of Chemistry

www.ksu.edu.sa
www.sciencedirect.com

ORIGINAL ARTICLE

One-pot *in-situ* hydrothermal synthesis of $VSe_2/MoSe_2$ nanocomposite for enhanced hydrogen evolution reaction

M. Alahmadi *, **Sami Ben Aoun** *

Chemistry Department, College of Science, Taibah University, P.O. Box 30002, Al-Madinah Al-Munawarah, Saudi Arabia

Received 10 January 2023; accepted 21 March 2023
Available online 27 March 2023

KEYWORDS

Hydrothermal synthesis;
VSe_2;
$MoSe_2$;
Nanocomposite;
Hydrogen evolution reaction;
Screen-printed electrodes

Abstract Hydrogen is the kind of pure, renewable energy that is required for the world to begin relying less and less on the fossil fuels that it currently consumes. The production of hydrogen by electrocatalytic water splitting is deemed to be preferable to the consumption of fossil fuels for the generation of clean and reliable energy. A catalyst's ability to catalyze is significantly influenced by the number of exposed active sites in the catalyst. Thus, the purpose of the current work is to offer a simple and inexpensive strategy to synthesize a double non-noble metal catalyst of $VSe_2/MoSe_2$ via one-step hydrothermal synthesis for catalytic Hydrogen evolution reaction (HER). The strong and unique orientation interaction between the nanosheet-like structure of VSe_2 and the nanoflower-like structure of $MoSe_2$ in the nanocomposite significantly improved the electron transfer kinetics. Subsequently, the electrochemical hydrogen production performance of the hybrid $VSe_2/MoSe_2$ is enhanced as compared to its constituent materials. Electrochemical characterizations prove that the $VSe_2/MoSe_2$ nanocomposite enhances the electrochemical activity performance with the lowest onset potential (330 mV) and a low value of Tafel plot (66 mV/decade) in comparison with sole $MoSe_2$ and VSe_2. In addition, the nanocomposite shows a low charge transfer resistance of 65 Ω, which further advocates the HER polarization curve and Tafel plot.

1. Introduction

The development of clean, sustainable and eco-friendly energy has attracted a lot of attention. Due to the rise in environmental degradation and the depletion of fossil resources, this interest is escalating speedily. The environmentally friendly electrochemical production of hydrogen through electrolysis of water ($2H_2O \rightarrow 2H_2 + O_2$) is a desirable option to produce a clean, sustainable and environmentally safe energy source compared to fossil fuels (Huang et al., 2018; Q. Zhang et al., 2020; Liang et al., 2015). Despite the fact that platinum and platinum-based alloys are the most efficient catalysts for the hydrogen evolution reaction (HER) in both acidic and alkaline conditions, their

* Corresponding authors.
E-mail addresses: mnahmadi@taibahu.edu.sa (M. Alahmadi), sbenaoun@taibahu.edu.sa (S. Ben Aoun).

Peer review under responsibility of King Saud University.

Production and hosting by Elsevier

https://doi.org/10.1016/j.arabjc.2023.104846
1878-5352

applicability in practical applications has been hampered by their intrinsic drawback of scarcity, high cost and low reserves (X.-D. Wang et al., 2016; Zhu et al., 2016; K. Zhang et al., 2015). Hence, the question of the development of alternative electrocatalysts that are non-precious, durable and highly HER active, as an alternative to Pt-based materials, is a crucial topic for scientists.

More recently, researchers have made enormous efforts to develop a variety of approaches to alternate precious electrocatalysts. Among these approaches, transition metal dichalcogenides (TMDC), including VSe_2, VS_2, WSe_2 and $MoSe_2$, have currently attracted a lot of interest due to their earth-abundant nature, unique structure and physical properties (Chen et al., 2018; Chhowalla et al., 2013; Alahmadi et al., 2021). TMDC consist of three layers (MX_2) bonded via Van der Waals forces, in which the middle layer is a transition metal (M) while the top and bottom layers are chalcogenide atoms (X) (Eichfeld et al., 2015; Fang et al., 2021; Fan et al., 2015).

Among various TMDC, molybdenum diselenide ($MoSe_2$) and its hybrids have been on the focus of research as electrocatalysts for HER due to their low cost, nontoxicity and ease of production. $MoSe_2$ material possesses two phases: the 2H (semiconducting) and the IT (metallic) set it apart from other TMDC materials (Kiran et al., 2014). Very recent reports have theoretically and experimentally demonstrated that the edge of materials controls the electronic structure. For instance, Jaramillo *et al.* and Helveg *et al.* have experimentally demonstrated through a scanning tunneling microscope (STM) that the active sites of MoS_2 layers are located along the edges of the domains while basal surfaces of the domains are inactive (Jaramillo et al., 2007; Helveg et al., 2000). In another study, Tang et al. showed that the atomic hydrogen adsorption on the $MoSe_2$ edges exhibits lower Gibbs free energy compared to MoS_2, which leads to greater coverage of hydrogen adsorption (Tang et al., 2014). Consequently, by tuning and manipulating the morphology of the nanoparticles or the sheets, by increasing the number of exposed active edge sites in TMDC, HER performance can be enhanced (Li et al., 2011; Poorahong et al., 2017; Liao et al., 2013). In addition, the influence of the electrocatalyst's electrical conductivity is a significant factor in HER activity. Thus, $MoSe_2$ is incapable of serving as a standalone and effective HER catalyst due to its poor conductivity and worse electroactive site exposure (Xu et al., 2018). Several attempts have been made to address this serious problem by employing strategies such as functional structure design (Ojha et al., 2017), synthesized hybrid materials (Tang et al., 2014) and doping with other materials (Deng et al., 2017; Qian et al., 2019). It is possible to alter the catalytic activity of $MoSe_2$ through the hybridization process, which is a simple technique for improving HER performance. Vanadium diselenide (VSe_2) has been cited in the literature as one of the most important TMDs, with special mention made of its exceptional properties, such as excellent electrocatalytic activities (Z.-L. Liu et al., 2018), high conductivity (Yi et al., 2022), charge density wave (Duvjir et al., 2018) and ferromagnetism (Bonilla et al., 2018). Moreover, VSe_2 is frequently used to modify the electronic structure when combined with other materials, thus reducing their overpotential (Kwon et al., 2022; Feng et al., 2022).

So far, successful techniques have been reported to increase the active edge sites of TMDCS including chemical deposition (H. Yang et al., 2016; Y. Zhang et al., 2015), electro-Fenton processing (Li et al., 2014), electrodeposition (Kuo et al., 2020), liquid exfoliation (Gopalakrishnan et al., 2014) and microwave heating process (Chen et al., 2019; Tang et al., 2021; Chen et al., 2020). These processes are frequently constrained because they require a lot of time, demand difficult circumstances, or involve the use of dangerous and expensive organic solvents (Ren et al., 2015). Among these methods, hydrothermal synthesis provides a lot of benefits for the economy and the environment (Chen et al., 2022).

In the current work, we demonstrated a facile one-pot synthesis strategy of the $VSe_2/MoSe_2$ nanocomposite by using a one-step hydrothermal method. In this method, we utilized ammonium molybdate hexahydrate precursor and vanadium nitrate as a metal source and selenium as a chalcogenide source for the one-pot growth of the $VSe_2/MoSe_2$ hybrid structure. The interaction between $MoSe_2$ and VSe_2, which is generally caused by the abundance of the $MoSe_2$ and VSe_2 interfaces, results in an increase in the number of catalytic active sites in the resulting hybrid heterostructure. The typical 3D heterostructure can enhance the active sites to fully expose in electrolyte due to the VSe_2 and $MoSe_2$ being well dispersed. In comparison to standalone pure VSe_2 and $MoSe_2$, the $VSe_2/MoSe_2$ hybrid displays better HER performances. The unique heterostructure of the $VSe_2/MoSe_2$ nanocomposite shows an excellent HER performance with a low onset potential of 330 mV, a small Tafel slope of 66 mV/decade, and excellent long-term stability in acidic medium. The structure, composition and morphology of the heterojunction nanocomposite were also studied using different characterization tools.

2. Materials and method

2.1. Chemical and reagents

Ammonium molybdate tetrahydrate ($(NH_4)\ Mo_7O_{24}{\cdot}6H_2O$), ammonium metavanadate (NH_4VO_3), oxalic acid ($C_2H_2O_4$), selenium (Se) and nafion solution (5 wt%) were obtained from Sigma-Aldrich. There was no additional purification performed for any of the chemicals and reagents.

2.2. Synthesis of $VSe_2/MoSe_2$ nanocomposite

We describe a facile and low-cost one-step hydrothermal technique that was employed to produce the $VSe_2/MoSe_2$ nanocomposite. In a typical synthesis, 40 ml of distilled water was used to dissolve 0.16 g of NH_4VO_3, 1.12 g of $C_2H_2O_4$ and 0.25 g of $(NH_4)\ Mo_7O_{24}{\cdot}6H_2O$. Following that, 0.16 g of Se powder was gradually added to the above solution as a source of a selenium precursor. Then, the resultant mixture was stirred for 1 h at ambient temperature. Subsequently, the solution was placed into a stainless steel autoclave and heated for 24 h at 200 °C. The mixture was allowed to cool at ambient temperature after the hydrothermal reaction. Finally, ethanol and distilled water were used to wash the synthesized products before being filtered using a filter paper. Finally, the synthesized product was dried for 12 h at 50 °C. For comparison, under the same conditions, both $MoSe_2$ and VSe_2 were also synthesized in their pure forms.

2.3. Materials characterization

The phase structure of the investigated samples was identified using X-ray powder diffraction (XRD) on a SHIMADZU-MAXima-XRD-7000 diffractometer equipped with Cu-Ka radiation (1.5418 A). Raman spectra of powder samples were performed on Senterra with a laser excitation wavelength of 532 nm. The structural phase of $VSe_2/MoSe_2$ was examined by X-ray photoelectron spectra (XPS) using K-alpha (Thermo fisher scientific, USA) with monochromatic X-ray Al K-Alpha radiation-10 to 1350ev spot size 400 μm at a pressure of 10^{-9} mbar. The morphology of the products was examined using filed emission scanning electron microscopy (FESEM-JSM-IT700HR). To examine the chemical composition of the developed hybrid nanocomposites, the energy dispersive X-ray (EDX) was also collected using the JSM-IT700HR. The hybrid $VSe_2/MoSe_2$ material was investigated using transmission electron microscopy (TEM) (QUANTA FEG 250).

2.4. Electrochemical measurements

All measurements of the electrochemistry were achieved by using Autolab (PGSTAT204) and recorded at room temperature. A disposable three-electrode conformation (screen printed carbon electrode (SPCE), Metrohm) consists of a working electrode (carbon), reference electrode (Ag/AgCl) and counter electrode (carbon). All experiments were performed in sulfuric acid (H_2SO_4, 0.5 M) as an electrolyte. All potentials in the present work are reported with respect to reversible hydrogen electrode RHE using the equation: $E_{RHE} = E_{Ag/AgCl} + 0.1976 + 0.056pH$. In order to make the catalyst ink, 55 mg of the catalyst material as it had been synthesized was dissolved in 4 ml solution of water-n-propanol (1:3). Then the catalyst ink was ultrasonicated for at least one hour in order to obtain a homogenous ink. Thereafter, 2 μL aliquot of the above slurry ink was directly drop-casted onto the 4 mm diameter working electrode and then covered with 2 μL of Nafion solution (1:3 water and propanol). Further, 10 ml of electrolyte (0.5 M H_2SO_4) was purged with nitrogen for at least 20 mins. Prior to evaluating the electrocatalytic activity of the $VSe_2/MoSe_2$ catalyst, a few cycles of cyclic voltammetry (CV) were performed to insure the electrode activation. Linear sweep voltammetry (LSV) was performed in 0.5 M H_2SO_4 by sweeping the potential in the range from 0.2 to −0.8V vs. RHE at a scan rate of 1 mV/s under nitrogen atmosphere. Electrochemical impedance spectroscopy (EIS) experiments were performed with frequency ranging from 80KHz to 1 Hz at a potential of 60 mV. To assess durability, 1000 cycles of the CV measurements were swept from 0.2 to −0.8 V at a scan rate of 100 mV/s.

3. Results and discussion

3.1. Structure and morphology of the nanocomposites

Using a simple one-pot hydrothermal procedure and common reagents like ammonium metavanadate, ammonium molybdate tetrahydrate, oxalic acid and selenium powder as precursors, the distinctive hierarchical solid blocks nanocomposite of $VSe_2/MoSe_2$ were synthesized. During our hydrothermal process, the VSe_2 prefers to produce ultra-thin nanosheets with random shapes while the $MoSe_2$ forms a nanoflower-like structure. Nevertheless, the $VSe_2/MoSe_2$ hybrid would lead to multidirectional solid blocks that are arranged in a hierarchy. Fig. 1 shows the XRD patterns and Raman spectra of the synthesized samples. Fig. 1(a) shows the XRD patterns of pure $MoSe_2$, VSe_2 and the hybrid mixture of $MoSe_2/VSe_2$. For the XRD pattern of the produced $MoSe_2$, all the diffraction peaks are perfectly consistent with the hexagonal $MoSe_2$ phase (JCPDS Card No. 77-1715). The reflection peaks localized at 14.6°, 37.06°, 44.4° and 66.2° corresponding to (002), (100), (103), (110), (105), and (110) planes, indicating excellent purity of the synthesized $MoSe_2$ (Liu et al., 2015). From the VSe_2 XRD patterns, the location of diffraction peaks is consistent with hexagonal VSe_2 nanosheets (DB Card No. 1538289, $a = b = 3295$ Å and $c = 6031$ Å). A few peaks at 2 theta of 14.4, 29.5, 32.4, 40.0, 43.5, 55.8, 60.0, 65.0, 71.4 and 86.3 originated from (001), (002), (011), (102), (003), (103),

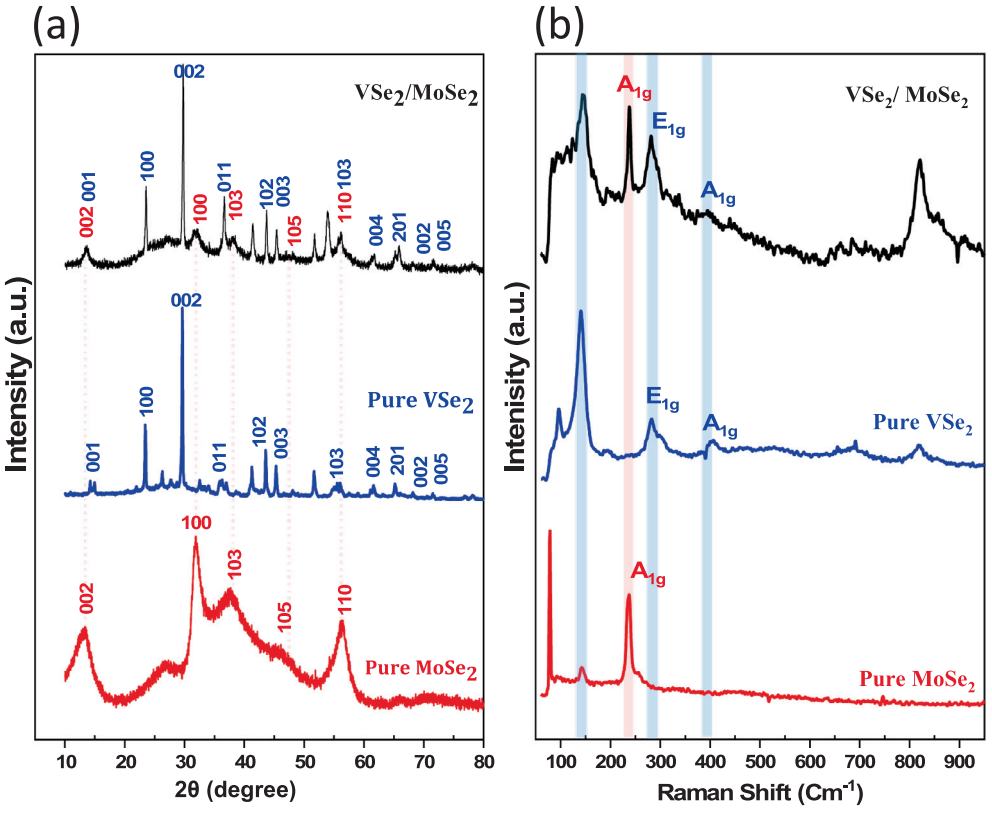

Fig. 1 (a) XRD patterns (b) Raman spectra of the as-synthesized materials of $MoSe_2$, VSe_2, and $VSe_2/MoSe_2$.

(004), (201), (002) and (005) planes (Sundaresan et al., 2023; He et al., 2017). For the $VSe_2/MoSe_2$ hybridized sample, all diffraction peaks of pure $MoSe_2$ and VSe_2 were observed. Further, Raman spectroscopy was employed to characterize the synthesized samples as shown in Fig. 1(b). The Raman spectra of $MoSe_2$ displays that the typical strong peak at 239 cm^{-1} corresponds to the A_{1g} out-of-plane vibration mode of the $MoSe_2$ (Yang et al., 2017; Huang et al., 2014). From the Raman profile of pure VSe_2, the vibration modes at 280 and 406 cm^{-1} are attributed to the vibration modes of E_{1g} and A_{1g}, respectively (Ming et al., 2018; Ratha et al., 2019). Raman spectra of the $VSe_2/MoSe_2$ mixture heterostructure exhibits the characteristic Raman bands of both sole $MoSe_2$ and VSe_2. The peaks at 280 and 406 cm^{-1} correspond to E_{2g} and A_{1g} vibration modes of VSe_2, respectively, while the A_{1g} vibrational mode of $MoSe_2$ is at 239 cm^{-1} implyes the existence of two materials in the heterostructure, which is also compatible with EDX and XPS analyses. These findings suggest that no phase shifts occurred during the synthesis of a nanocomposite comprised of $MoSe_2$ and VSe_2.

The morphology and nanostructure of the pristine VSe_2 and $MoSe_2$ structures as well as the $VSe_2/MoSe_2$ nanocomposite were studied using field emission scanning electron microscopy (FESEM). As exhibited in Fig. 2(a), the pristine VSe_2 shows a nanosheet-like structure with a length of a few micrometers. On closer inspection, it becomes clear that these VSe_2 are made of a number of ultrathin nanosheets, with an estimated thickness of each nanosheet of roughly 10 nm (Fig. 2(b). Fig. 2(c) and Fig. 2(d) show the nanoflower-like structures of the pure $MoSe_2$ that were synthesized through the hydrothermal method from (NH_4) $Mo_7O_{24}{\cdot}6H_2O$ and Se. It is composed of ultrathin nanosheets with an average thickness of roughly 20 nm. The morphology of the hybrid $VSe_2/MoSe_2$ is illustrated in Fig. 2(e) and Fig. 2(f). It has been observed that when using combinations of V and Mo salts under the same experimental conditions, the produced $VSe_2/MoSe_2$ nanocomposites display morphologies that are completely different from either VSe_2 or $MoSe_2$. As clearly observed, the nanocomposite forms a hierarchical slab-stacking-like structure. Further, the elemental composition of the hybrid $VSe_2/MoSe_2$ nanocomposite was also examined using an EDX analysis, as revealed in Fig. 2(g), identifying Mo, V and Se as the primary constituents of the synthesized nanocomposite. The presence of these elements is further confirmed by EDX elemental mapping (Fig. 2(i-k)), which is also distributed throughout the hybrid composite material. Meanwhile, VSe_2 and $MoSe_2$ in the hybrid mixture seem to be in close contact based on the distribution of Mo, V, and Se.

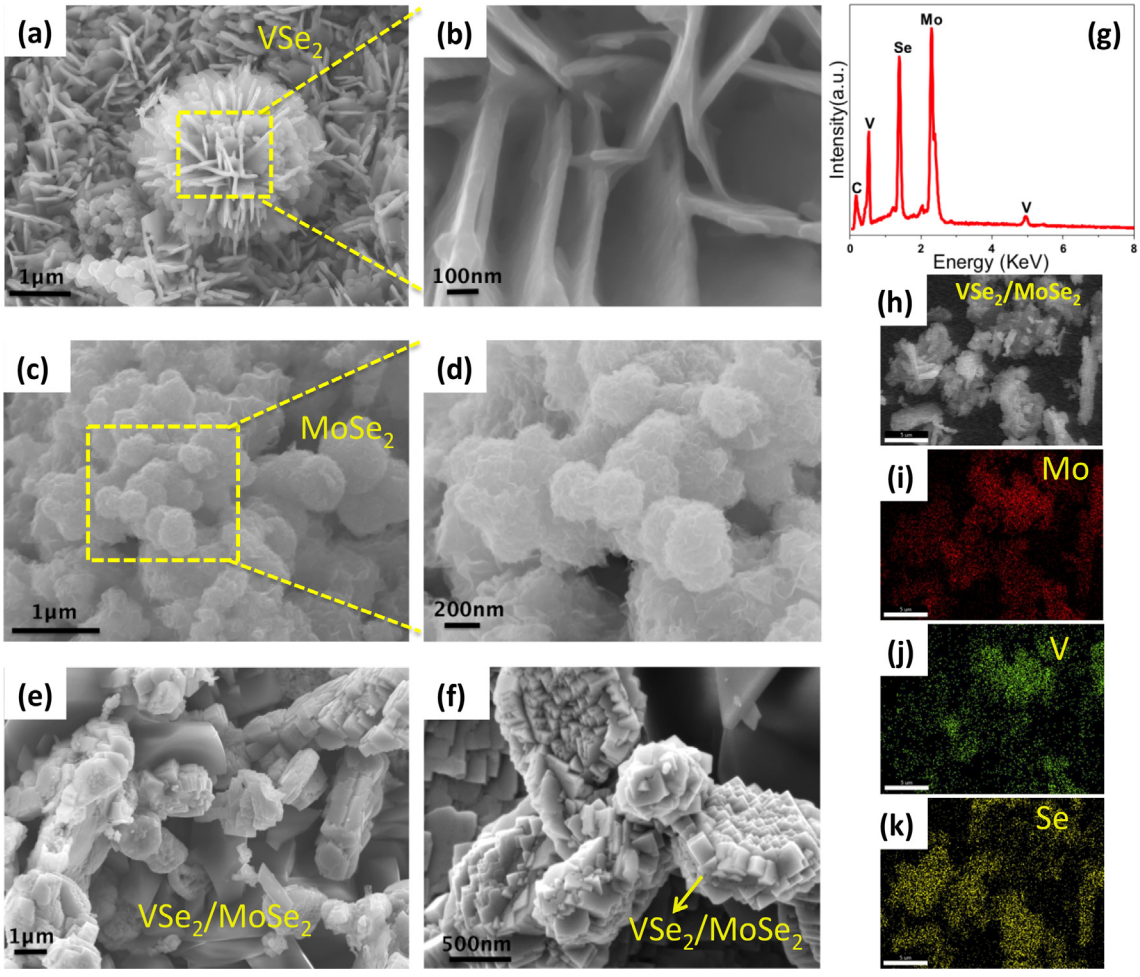

Fig. 2 (a and B) FESEM images of pristine VSe_2 nanosheets at different magnifications, (c and d) flower-like structure of $MoSe_2$, (e and f) hybrid $VSe_2/MoSe_2$ material, (g) EDX spectra of $VSe_2/MoSe_2$ and (i-k) element mapping images of Mo, V, and Se, respectively.

These findings indicate that the $VSe_2/MoSe_2$ hybrid nanostructure was successfully synthesized and contains both components. The hybrid $VSe_2/MoSe_2$ exhibits two distinct types of lattice fringes in high-resolution TEM analyses, as shown in Fig. 3(a) and (b). The interplanar spacing of the $MoSe_2$ (0 0 2) plane is 0.63 nm (Wu et al., 2020) while the interplanar spacing of the VSe_2 (0 1 1) plane is 0.263 nm (KA et al., 2020).

To confirm the surface chemical composition of the $VSe_2/MoSe_2$ heterostructure and the purity of its VSe_2 and $MoSe_2$ constituents, high-resolution X-ray photoelectron spectroscopy (XPS) measurements were made. The survey scan spectrum of $MoSe_2$, VSe_2, and $VSe_2/MoSe_2$ nanostructures is illustrated in Fig. 4(a). The synthesized samples mainly contain the five elements V, Mo, Se, C and O. The major source of the C 1S signal at 284.6 eV is the contamination from the carbon conductive tape that was used to hold the sample for the XPS analysis. The O 1 s signal in the XPS survey scan implies the existence of oxide phases that may be caused by the surface adsorption of oxygen. Moreover, as shown in Fig. 4(b), the pristine VSe_2 nanostructure shows two distinct peaks, which are attributed to V $2p_{3/2}$ and V $2p_{1/2}$, localized at binding energies of 517.15 and 523.5 eV, respectively. The peak at about 517.15 eV suggests the occurrence of V^{4+} (+4 oxidation state of vanadium) (Ulusoy Ghobadi et al., 2017; Karamat et al., 2016). In the $VSe_2/MoSe_2$ nanocomposite, this peak was also shifted to a low-binding energy region as a result of the incorporation of $MoSe_2$. The $VSe_2/MoSe_2$ spectrum, as shown in Fig. 4(c), has four dominant peaks. The two peaks at 229.7 and 232.8 eV, which correspond to Mo $3d_{5/2}$ and Mo $3d_{3/2}$, are assigned to the oxidation state of the Mo^{4+}. The peaks located at 230.8 and 235.5 eV, which correspond to Mo $3d_{5/2}$ and Mo $3d_{3/2}$, are assigned to the oxidation state of the Mo^{6+}(J. Yang et al., 2016; Zhang et al., 2018). These confirmed that Mo is mainly present in the nanocomposite mixture before being oxidized (L. Zhang et al., 2020). Additionally, the former small peak at around 235.5 eV indicates the presence of the hexavalent state of Mo, which is assigned to Mo $3d_{3/2}$. On the other hand, in the case of pure $MoSe_2$, the hexavalent state peak becomes barely detectable. This peak indicates the reduction of Mo of the hexavalent state (Mo (VI) $3d_{3/2}$, 235.5 eV) to the tetravalent state (Mo (IV) $3d_{5/2}$, 232.5 eV) (Wang et al., 2014). Further, the binding energies of Mo (IV) $3d_{3/2}$ shift by 0.5 eV, indicating that the electronic structure of $MoSe_2$ in the nanocomposite has been modified. The hexavalent state peak may be most likely caused by a combination of factors, including the reduction of MoO_4^{-2} during the hydrothermal reaction (Sakthivel et al., 2018), air oxidation of the $MoSe_2/VSe_2$ surface (Fan et al., 2015), or the formation of vacancies in the VSe_2 structure in the hybrid structure. It is noteworthy that by utilizing thermal treatment annealing at a high temperature of 600 °C, this peak can be completely eliminated (Zhang et al., 2017). In a comparable kind of this application, *Zhang et al.* have also realized this peak (L. Zhang et al., 2020). Further, Fig. 4(d) displays the XPS analysis of Se 3d. For hybrid $VSe_2/MoSe_2$ material, the characteristic doublet peaks are referred to Se $3d_{5/2}$ at 55 eV and Se $3d_{3/2}$ at 56.3 eV, indicating the −2 oxidation state of selenium (H. Yang et al., 2016). These findings support the successful synthesis of pure VSe_2, $MoSe_2$ and hybrid composites.

3.2. Electrocatalytic analysis

We evaluated the electrocatalytic performances of modified SPCE with the as-prepared $MoSe_2$, pristine VSe_2 and $VSe_2/MoSe_2$ nanocomposite in 0.5 M H_2SO_4 solution by LSV with a scan rate of 1 mVs^{-1} at ambient temperature. The electrochemical performance of Pt was also studied as a control experiment. The prepared electrocatalysts will be denoted as $MoSe_2$@SPCE, VSe_2@SPCE and $VSe_2/MoSe_2$@SPCE, respectively. The polarization curves are shown in Fig. 5(a). Among all three electrocatalysts, the $VSe_2/MoSe_2$@SPCE exhibits the highest HER catalytic activity with an onset potential of 330 mV revealing robust interaction in the interface that could develop the activity. Comparatively, $MoSe_2$@-SPCE and VSe_2@SPCE exhibit higher overpotentials. Due to the lower electrocatalytic reduction of proton to H_2, the cathodic current rose under more negative potential. Consequently, a relatively low hydrogen evolution activity was observed. It is noteworthy that the one-pot synthesed $VSe_2/MoSe_2$ can be stated as having better catalytic activity. With the one-pot synthesis method, we think there are unique possibilities for enhancing the catalytic activity of dual non-noble materials.

The Tafel slope, which can use to understand the dynamics of hydrogen evolution and reaction mechanism, is extracted from the polarization curves (Shi et al., 2017; Yan et al., 2017). From the Tafel equation ($\eta = b \log(j) + a$) (Begum et al., 2023), where η is the overpotential, b is the Tafel slope and j is the current density, the Tafel slope is derived. In order

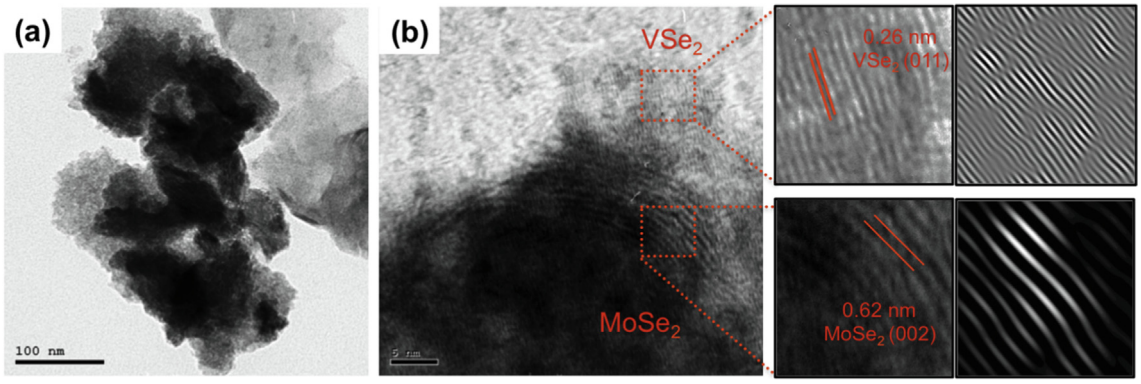

Fig. 3 (a and b) TEM images of the hybrid $VSe_2/MoSe_2$ material with the d spacing of VSe_2 and $MoSe_2$ and with the corresponding lattice scale views.

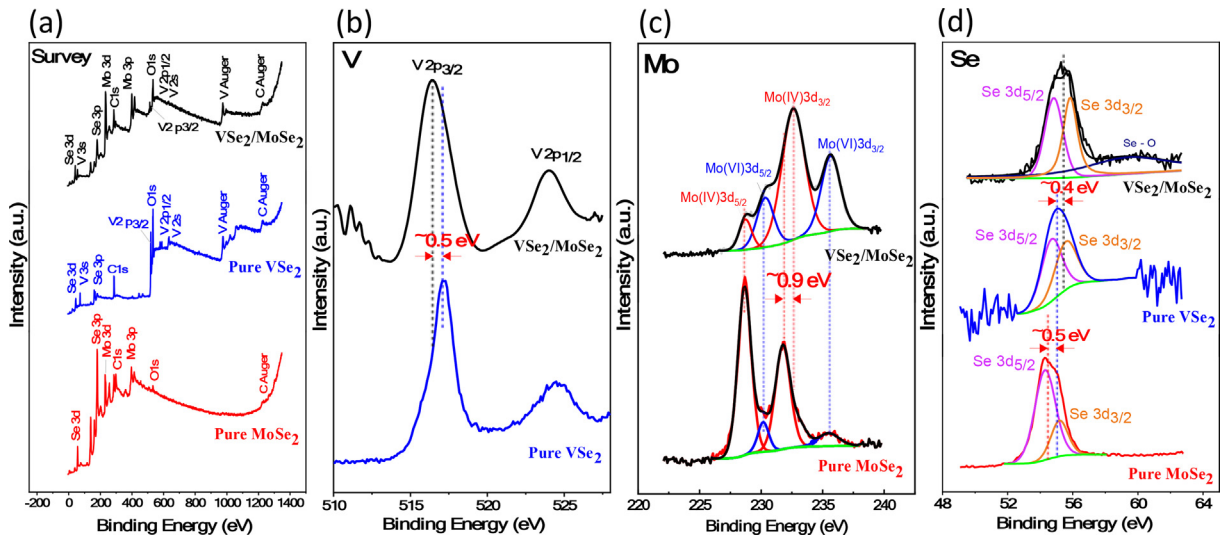

Fig. 4 XPS spectra of the hybrid $VSe_2/MoSe_2$ product: (a) XPS survey spectra of $MoSe_2$, VSe_2 and $VSe_2/MoSe_2$, (b) XPS spectra of Mo 3d, (c) V 2p, and (c) Se 3d,respectively.

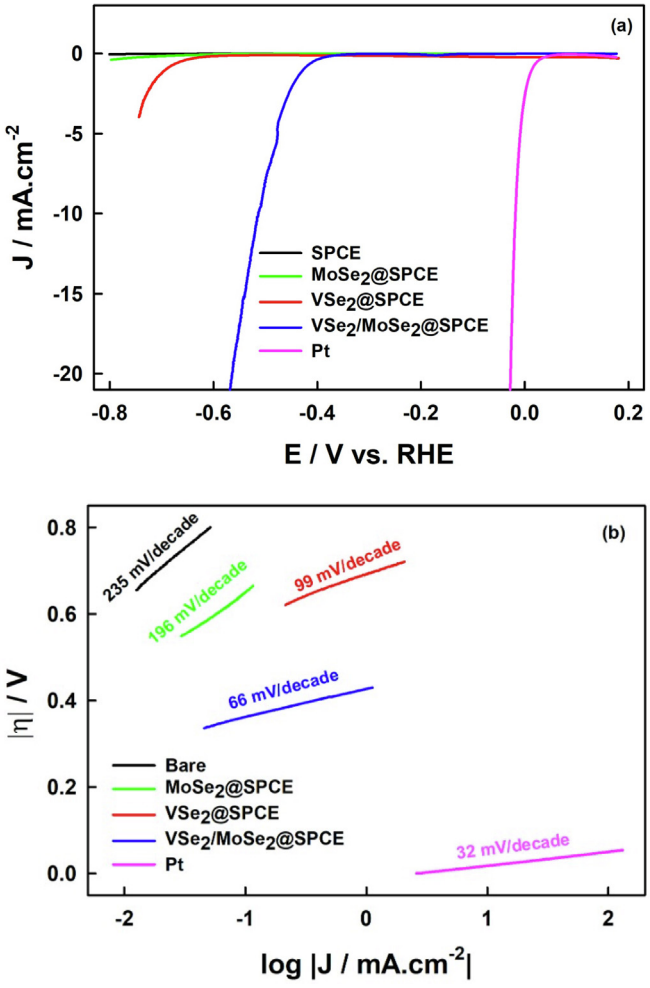

Fig. 5 (a) The HER polarization curves of $MoSe_2$@SPCE, VSe_2 @SPCE and hybrid $VSe_2/MoSe_2$@SPCE in 0.5 M H_2SO_4. (b) Tafel Plots derived from the HER polarization curves.

to estimate the Tafel slope of the various electrocatalysts, Tafel plots are reported in Fig. 5(b). A Tafel slope of 66 mV decade^{-1} is determined for $VSe_2/MoSe_2$@SPCE. This value indicates that the hybrid nanocomposite increases the HER catalytic activity since it is substantially lower than the value observed for VSe_2@SPCE (99 mV decade^{-1}), $MoSe_2$@SPCE (196 mV decade^{-1}) and bare SPCE (235 mVdecade^{-1}). Interestingly, the Tafel slope value of $VSe_2/MoSe_2$@SPCE is lower compared to other TMDC previously reported; like $MoSe_2$/Graphene (80 mVdecade^{-1}; Najafi et al., 2018), MoS_2 nanosheets (90 mVdecade^{-1}; Muralikrishna et al., 2015) and WSe_2/rGO (85 mVdecade^{-1}; Li et al., 2018).

Understanding the interfacial processes of the $VSe_2/MoSe_2$ hybrid material requires an examination of the kinetics of HER. *Conway et al.* revealed a well-known conclusion regarding the participation of chemisorbed hydrogen, which may help in understanding how the cathodic H_2 evolution reaction occurs at electrodes (Conway and Tilak, 2002; Conway and Tilak, 1992; Tilak et al., 1977; X. Wang et al., 2016). Typically, the HER includes three main steps to convert H^+ to H_2 in acidic electrolytes.

$$H_3O^+ + e^- + M \rightarrow MH_{ads} + H_2O \ \ (step\ 1,\ \ Volmer\ \ reaction) \quad (1)$$

$$MH_{ads} + H_2O^+ + e^- \rightarrow H_2 + H_2O \ \ (step\ 2, Heyrovsky\ \ reaction) \quad (2)$$

$$2MH_{ads} \rightarrow 2M + H_2 \ \ (step\ 3, Tafel\ \ reaction) \quad (3)$$

Where M denotes the catalyst while M_{Hads} denotes the hydrogen atom adsorbed on the surface of the catalyst. The first step (1) is known as a discharge step (Volmer step, 120 mV dec^{-1}). Herein, hydrogen ions (H_3O^+) and electrons interact to form adsorbed hydrogen intermediates (M_{Hads}) on the surface of the catalyst. The following steps (2 or 3) are desorption, also known as Heyrovsky electrochemical reaction (40 mV dec^{-1}) or Tafel chemical reaction (30 mV dec^{-1}). In the current work, the hybrid VSe_2/MSe_2 material has a Tafel slope of 66 mVdec^{-1}, which indicates that the Volmer and Heyrovsky reactions are taking place during the HER activity. In contrast to pure VSe_2 and MSe_2, the lower Tafel slope of VSe_2/MSe_2 should be the result of the H intermediate participating in a different state, which is promoted by the disordered state of the surface of VSe_2/MSe_2.

In order to further explore the relationship between the active surface of the electrocatalysts and catalytic HER activity, the charge-transfer processes of the various electrocatalysts were studied by (EIS) (Argoubi et al., 2015, 2019; Mars et al.,

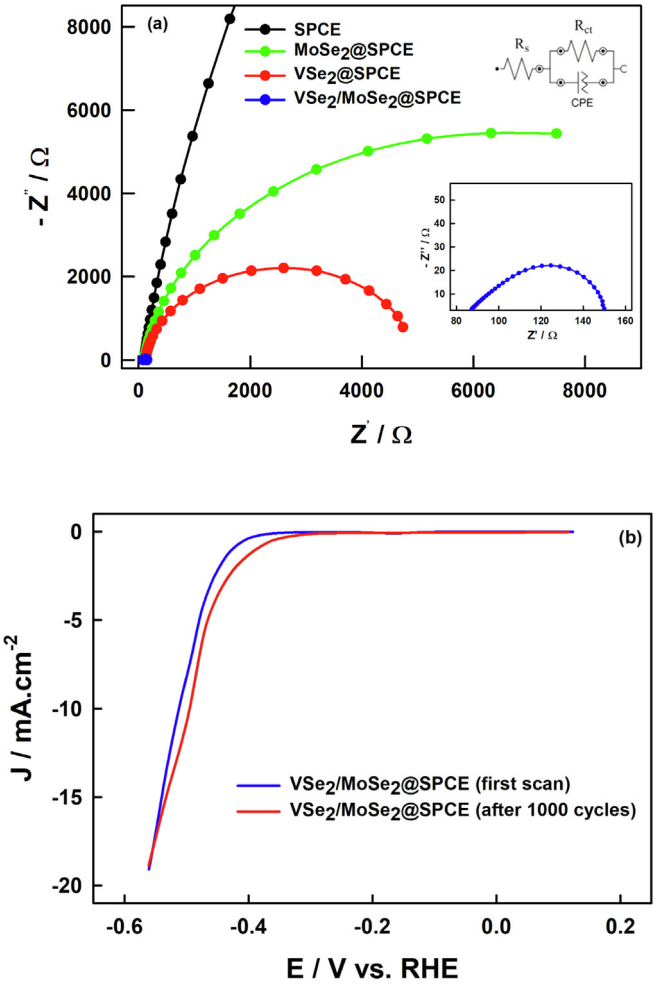

Fig. 6 (a) Nyquist plots of $MoSe_2$@SPCE, VSe_2@SPCE and $VSe_2/MoSe_2$@SPCE in 0.5 M H_2SO_4. (b) Stability results of the $VSe_2/MoSe_2$@SPCE before and after 1000 CV cycles in 0.5 M H_2SO_4.

Table 1 Comparison Table of various MoSe2 and MoSe2-based electrocatalysts.

HER catalyst	Synthesis technique	Loading	Electrolyte	Tafel slope mV/dec	Overpotential η10 (mV)	Resistance	Reference
$MoSe_2$/GC	LPA	2 mg cm^{-2}	0.5 M H_2SO_4	88	−340	–	(Najafi et al., 2018)
$MoSe_2$/CNFs	CVD	–	0.5 M H_2SO_4	107	−219	–	(H. Yang et al., 2016)
Porous $MoSe_2$	Liquid Exfoliation Method	0.45 mg cm^{-2}	0.5 M H_2SO_4	80	−150	25	(Lei et al., 2016)
$MoSe_2$/WSe_2	Colloidal Method	0.28 mg cm^{-2}	0.5 M H_2SO_4	238	−580	713	(Hwang and Shin, 2021)
$MoSe_2$-NiSe@C	Hydrothermal Synthesis	0.25 mg cm^{-2}	0.5 M H_2SO_4	76.3	−154	–	(C. Liu et al., 2018)
H-$NiSe_2$/$MoSe_2$	Hydrothermal Synthesis	0.6 mg cm^{-2}	0.5 M H_2SO_4	43.5	−147	188.2	(Dai et al., 2022)
Co doped $MoSe_2$	Hot Injection Technique	1.04 mg cm^{-2}	0.5 M H_2SO_4	67	−232	388	(Zimron et al., 2020)
VSe_2/$MoSe_2$@SPCE	**Hydrothermal Synthesis**	**0.2 mg cm^{-2}**	**0.5 M H_2SO_4**	**66**	**−480**	**65**	**This Work**

2016; Aoun, 2017). Fig. 6(a) shows the obtained Nyquist plot of $MoSe_2$@SPCE, VSe_2 @SPCE and VSe_2/$MoSe_2$@SPCE electrocatalysts along with bare SPCE. The charge transfer resistance (R_{ct}) of the electrocatalysts is a typical parameter reflecting the interfacial Faradic kinetics of the catalytic reaction of HER. Calculations were made based on the best fitting of the experimental data using a simple Randles-type equivalent circuit (Tanjila et al., 2021) (cf. inset of Fig. 6(a)). The VSe_2/$MoSe_2$@SPCE has the lowest R_{ct} value of 65 Ω while those of VSe_2@SPCE and $MoSe_2$@SPCE are around 4.84 and 12.50 kΩ, respectively. Additionally, the low resistance of the VSe_2/$MoSe_2$ hybrid material implies a highly effective electrical communication between the two catalytic edge sites. This tremendous decrease in charge transfer means a substantially greater conductivity of the VSe_2/$MoSe_2$@SPCE. This goes in line with the observed superior HER performance revealed from the polarization measurements. Moreover, along with its outstanding electrocatalytic activity, the durability is another essential factor to be considered. As presented in Fig. 6(b), the long-term stability of the VSe_2/$MoSe_2$@SPCE electrocatalyst was evaluated upon 1000 uninterrupted CV cycles in 0.5 M H_2SO_4 after 4 months of storage. In fact, the VSe_2/$MoSe_2$@SPCE electrocatalyst demonstrated excellent long-term stability with a minor drop in current densities and an even slightly positively shifted HER onset potential. This finding indicates the excellent stability of the VSe_2/$MoSe_2$ catalyst throughout HER performance. Table 1 provides a thorough comparison of several catalysts in terms of the synthesis process, electrolyte, charge transfer resistance and Tafel slope. As illustrated in Table 1, our nanocomposite nanomaterials' resistance and Tafel slope are comparable or even better than those of previously reported $MoSe_2$-based nanocomposite nanomaterials.

4. Conclusion

In summary, we have presented insights into the synthesis of a simple and cost-effective HER catalyst (VSe_2/$MoSe_2$) using a one-pot hydrothermal technique. Such technique led to maximize surface area by raising the number of exposed edges of the VSe_2/$MoSe_2$ nanocomposite, which in turn improved the HER catalytic activity. The proposed VSe_2/$MoSe_2$@SPCE electrocatalyst exhibits a drastically reduced charge transfer towards HER facilitated by the strong interaction between VSe_2 and $MoSe_2$, which also increases the conductivity of the nanocomposite as a whole. The prepared electrocatalyst presented an outstanding HER activity with a relatively low onset potential of 330 mV and a small Tafel slope of 66 mV $decade^{-1}$. In addition, impedance analysis reveals a low charge transfer resistance of 65 Ω for the prepared VSe_2/$MoSe_2$@SPCE, which suggests that active edge sites are more numerous. Due to its excellent stability in an acidic medium, VSe_2/$MoSe_2$@SPCE would be a potentially sophisticated HER electrocatalyst.

Declaration of Competing Interest

The authors declare that they have no known competing financial interests or personal relationships that could have appeared to influence the work reported in this paper.

References

Alahmadi, M., Mahvash, F., Szkopek, T., Siaj, M., 2021. A two-step chemical vapor deposition process for the growth of continuous vertical heterostructure WSe 2/h-BN and its optical properties. RSC Adv. 11, 16962–16969.

Argoubi, W., Rabti, A., Aoun, S.B., et al, 2019. Sensitive detection of ascorbic acid using screen-printed electrodes modified by electroactive melanin-like nanoparticles. RSC advances 9, 37384–37390.

Argoubi, W., Saadaoui, M., Aoun, S.B., et al, 2015. Optimized design of a nanostructured SPCE-based multipurpose biosensing platform formed by ferrocene-tethered electrochemically-deposited cauliflower-shaped gold nanoparticles. Beilstein Journal of Nanotechnology 6, 1840–1852.

Begum, H., Islam, M.N., Ben Aoun, et al, 2023. Electrocatalytic reduction of nitrate ions in neutral medium at coinage metal-modified platinum electrodes. Environ. Sci. Pollut. Res. 30, 34904–34914. https://doi.org/10.1007/s11356-022-24372-z.

Ben Aoun, S., 2017. Nanostructured carbon electrode modified with N-doped graphene quantum dots–chitosan nanocomposite: a sensitive electrochemical dopamine sensor. Royal Society open science. 4, 171199.

Bonilla, M., Kolekar, S., Ma, Y., Diaz, H.C., Kalappattil, V., Das, R., Eggers, T., Gutierrez, H.R., Phan, M.-H., Batzill, M., 2018. Strong room-temperature ferromagnetism in VSe2 monolayers on van der Waals substrates. Nat. Nanotechnol. 13, 289–293.

Chen, Z., Chen, P., Xing, P., Hu, X., Lin, H., Wu, Y., Zhao, L., He, Y., 2018. Novel carbon modified KTa0. 75Nb0. 25O3 nanocubes with excellent efficiency in photocatalytic H2 evolution. Fuel 233, 486–496.

Chen, P., Chen, L., Ge, S., Zhang, W., Wu, M., Xing, P., Rotamond, T.B., Lin, H., Wu, Y., He, Y., 2020. Microwave heating preparation of phosphorus doped g-C3N4 and its enhanced performance for photocatalytic H2 evolution in the help of Ag3PO4 nanoparticles. Int. J. Hydrogen Energy 45, 14354–14367.

Chen, L., Wang, J., Li, X., Zhao, C., Hu, X., Wu, Y., He, Y., 2022. A novel Z-scheme Bi-Bi 2 O 3/KTa 0.5 Nb 0.5 O 3 heterojunction for efficient photocatalytic conversion of N 2 to NH. Inorg. Chem. Front.

Chen, P., Xing, P., Chen, Z., Hu, X., Lin, H., Zhao, L., He, Y., 2019. In-situ synthesis of AgNbO3/g-C3N4 photocatalyst via microwave heating method for efficiently photocatalytic H2 generation. J. Colloid Interface Sci. 534, 163–171.

Chhowalla, M., Shin, H.S., Eda, G., Li, L.-J., Loh, K.P., Zhang, H., 2013. The chemistry of two-dimensional layered transition metal dichalcogenide nanosheets. Nat. Chem. 5, 263–275. https://doi.org/10.1038/nchem.1589.

Conway, B.E., Tilak, B.V., 1992. Behavior and characterization of kinetically involved chemisorbed intermediates in electrocatalysis of gas evolution reactions. In: Advances in Catalysis. Elsevier, pp. 1–147.

Conway, B.E., Tilak, B.V., 2002. Interfacial processes involving electrocatalytic evolution and oxidation of H2, and the role of chemisorbed H. Electrochim. Acta 47, 3571–3594.

Dai, T., Sun, J., Peng, X., Gong, J., Zhou, Z., Wang, X., 2022. In situ synthesis of heterogeneous NiSe2/MoSe2 nanocomposite for high-efficiency electrocatalytic hydrogen evolution reaction. Energy Sci. Eng.

Deng, S., Zhong, Y., Zeng, Y., Wang, Y., Yao, Z., Yang, F., Lin, S., Wang, X., Lu, X., Xia, X., 2017. Directional construction of vertical nitrogen-doped 1T–2H MoSe2/graphene shell/core nanoflake arrays for efficient hydrogen evolution reaction. Adv. Mater. 29, 1700748.

Duvjir, G., Choi, B.K., Jang, I., Ulstrup, S., Kang, S., Thi Ly, T., Kim, S., Choi, Y.H., Jozwiak, C., Bostwick, A., 2018. Emergence of a metal–insulator transition and high-temperature charge-density waves in VSe2 at the monolayer limit. Nano Lett. 18, 5432–5438.

Eichfeld, S.M., Hossain, L., Lin, Y., Piasecki, A.F., Kupp, B., Birdwell, A.G., Burke, R.A., Lu, N., Peng, X., Li, J., Azcatl, A., Mcdonnell, S., Wallace, R.M., Kim, M.J., Mayer, T.S., Redwing, J.M., Robinson, J.A., 2015. Highly scalable, atomically Thin WSe2 grown via metal-organic chemical vapor deposition. ACS Nano 9, 2080–2087. https://doi.org/10.1021/nn5073286.

Fan, X., Xu, P., Zhou, D., Sun, Y., Li, Y.C., Nguyen, M.A.T., Terrones, M., Mallouk, T.E., 2015. Fast and efficient preparation of exfoliated 2H MoS2 nanosheets by sonication-assisted lithium intercalation and infrared laser-induced 1T to 2H phase reversion. Nano Lett. 15, 5956–5960.

Fang, B., Yao, J., Zhang, X., Ma, L., Ye, Y., Tang, J., Zou, G., Zhang, J., Jiang, L., Sun, Y., 2021. A large scaled-up monocrystalline 3R MoS 2 electrocatalyst for efficient nitrogen reduction reactions. New J. Chem. 45, 2488–2495.

Feng, W., Cheng, M., Du, R., Wang, Y., Wang, P., Li, H., Song, L., Wen, X., Yang, J., Li, X., 2022. Gram-scale synthesized two-dimensional VSe2 and SnSe2 for ultrahigh electrocatalytic sulfion recycling. Adv. Mater. Interfaces 9, 2200060.

Gopalakrishnan, D., Damien, D., Shaijumon, M.M., 2014. MoS2 quantum dot-interspersed exfoliated MoS2 nanosheets. ACS Nano 8, 5297–5303.

He, S., Lin, H., Qin, L., Mao, Z., He, H., Li, Y., Li, Q., 2017. Synthesis, stability, and intrinsic photocatalytic properties of vanadium diselenide. J. Mater. Chem. A 5, 2163–2171.

Helveg, S., Lauritsen, J.V., Lægsgaard, E., Stensgaard, I., Nørskov, J. K., Clausen, B.S., Topsøe, H., Besenbacher, F., 2000. Atomic-scale structure of single-layer MoS 2 nanoclusters. Phys. Rev. Lett. 84, 951.

Huang, J., Gao, H., Xia, Y., Sun, Y., Xiong, J., Li, Y., Cong, S., Guo, J., Du, S., Zou, G., 2018. Enhanced photoelectrochemical performance of defect-rich ReS2 nanosheets in visible-light assisted hydrogen generation. Nano Energy 46, 305–313.

Huang, C., Wu, S., Sanchez, A.M., Peters, J.J.P., Beanland, R., Ross, J.S., Rivera, P., Yao, W., Cobden, D.H., Xu, X., 2014. Lateral heterojunctions within monolayer MoSe2–WSe2 semiconductors. Nat. Mater. 13, 1–6. https://doi.org/10.1038/nmat4064.

Hwang, Y., Shin, N., 2021. Colloidal synthesis of MoSe2/WSe2 heterostructure nanoflowers via two-step growth. Materials (Basel). 14, 7294.

Jaramillo, T.F., Jørgensen, K.P., Bonde, J., Nielsen, J.H., Horch, S., Chorkendorff, I., 2007. Identification of active edge sites for electrochemical H2 evolution from MoS2 nanocatalysts. Science (80-.) 317, 100–102.

KA, S.R., Shajahan, A.S., Chakraborty, B., Rout, C.S., 2020. The role of carbon nanotubes in enhanced charge storage performance of VSe 2: experimental and theoretical insight from DFT simulations. RSC Adv. 10, 31712–31719.

Karamat, S., Rawat, R.S., Lee, P., Tan, T.L., Ke, C., Chen, R., Sun, H.D., 2016. Ferromagnetic signature in vanadium doped ZnO thin films grown by pulsed laser deposition. J. Mater. Res. 31, 3223–3229.

Kiran, V., Mukherjee, D., Jenjeti, R.N., Sampath, S., 2014. Active guests in the MoS 2/MoSe 2 host lattice: Efficient hydrogen evolution using few-layer alloys of MoS 2 (1–x) Se 2x. Nanoscale 6, 12856–12863.

Kuo, C.-W., Chang, J.-C., Wu, B.-W., Wu, T.-Y., 2020. Electrochemical characterization of RuO2-Ta2O5/polyaniline composites as potential redox electrodes for supercapacitors and hydrogen evolution reaction. Int. J. Hydrogen Energy 45, 22223–22231.

Kwon, I.S., Kwak, I.H., Zewdie, G.M., Lee, S.J., Kim, J.Y., Yoo, S.J., Kim, J.-G., Park, J., Kang, H.S., 2022. WSe2–VSe2 alloyed nanosheets to enhance the catalytic performance of hydrogen evolution reaction. ACS Nano 16, 12569–12579.

Lei, Z., Xu, S., Wu, P., 2016. Ultra-thin and porous MoSe 2 nanosheets: facile preparation and enhanced electrocatalytic activity towards the hydrogen evolution reaction. Phys. Chem. Chem. Phys. 18, 70–74.

Li, B.L., Chen, L.X., Zou, H.L., Lei, J.L., Luo, H.Q., Li, N.B., 2014. Electrochemically induced Fenton reaction of few-layer MoS 2 nanosheets: preparation of luminescent quantum dots via a transition of nanoporous morphology. Nanoscale 6, 9831–9838.

Li, J., Liu, P., Qu, Y., Liao, T., Xiang, B., 2018. WSe2/rGO hybrid structure: a stable and efficient catalyst for hydrogen evolution reaction. Int. J. Hydrogen Energy 43, 2601–2609.

Li, Y., Wang, H., Xie, L., Liang, Y., Hong, G., Dai, H., 2011. MoS2 nanoparticles grown on graphene: an advanced catalyst for the hydrogen evolution reaction. J. Am. Chem. Soc. 133, 7296–7299.

Liang, L., Cheng, H., Lei, F., Han, J., Gao, S., Wang, C., Sun, Y., Qamar, S., Wei, S., Xie, Y., 2015. Metallic single-unit-cell orthorhombic cobalt diselenide atomic layers: robust water-electrolysis catalysts. Angew. Chemie 127, 12172–12176. https://doi.org/10.1002/ange.201505245.

Liao, L., Zhu, J., Bian, X., Zhu, L., Scanlon, M.D., Girault, H.H., Liu, B., 2013. MoS2 formed on mesoporous graphene as a highly active catalyst for hydrogen evolution. Adv. Funct. Mater. 23, 5326–5333.

Liu, C., Wang, K., Zheng, X., Liu, X., Liang, Q., Chen, Z., 2018a. Rational design of MoSe2-NiSe@ carbon heteronanostructures for efficient electrocatalytic hydrogen evolution in both acidic and alkaline media. Carbon N. Y. 139, 1–9.

Liu, Z.-L., Wu, X., Shao, Y., Qi, J., Cao, Y., Huang, L., Liu, C., Wang, J.-O., Zheng, Q., Zhu, Z.-L., 2018b. Epitaxially grown monolayer VSe2: an air-stable magnetic two-dimensional material with low work function at edges. Sci. Bull. 63, 419–425.

Liu, Y., Zhu, M., Chen, D., 2015. Sheet-like MoSe 2/C composites with enhanced Li-ion storage properties. J. Mater. Chem. A 3, 11857–11862.

Mars, A., Argoubi, W., Aoun, S.B., et al, 2016. Induced conformational change on ferrocenyl-terminated alkyls and their application as transducers for label-free immunosensing of Alzheimer's disease biomarker. RSC advances 6, 2414–2421.

Ming, F., Liang, H., Lei, Y., Zhang, W., Alshareef, H.N., 2018. Solution synthesis of VSe2 nanosheets and their alkali metal ion storage performance. Nano Energy 53, 11–16.

Muralikrishna, S., Manjunath, K., Samrat, D., Reddy, V., Ramakrishnappa, T., Nagaraju, D.H., 2015. Hydrothermal synthesis of 2D MoS 2 nanosheets for electrocatalytic hydrogen evolution reaction. RSC Adv. 5, 89389–89396.

Najafi, L., Bellani, S., Oropesa-Nuñez, R., Ansaldo, A., Prato, M., Del Rio Castillo, A.E., Bonaccorso, F., 2018. Engineered MoSe2-based heterostructures for efficient electrochemical hydrogen evolution reaction. Adv. Energy Mater. 8, 1703212.

Ojha, K., Saha, S., Banerjee, S., Ganguli, A.K., 2017. Efficient electrocatalytic hydrogen evolution from MoS2-functionalized Mo2N nanostructures. ACS Appl. Mater. Interfaces 9, 19455–19461.

Poorahong, S., Izquierdo, R., Siaj, M., 2017. An efficient porous molybdenum diselenide catalyst for electrochemical hydrogen generation. J. Mater. Chem. A 5, 20993–21001.

Qian, J., Wang, T., Xia, B., Xi, P., Gao, D., 2019. Zn-doped MoSe2 nanosheets as high-performance electrocatalysts for hydrogen evolution reaction in acid media. Electrochim. Acta 296, 701–708.

Ratha, S., Bankar, P., Gangan, A.S., More, M.A., Late, D.J., Behera, J.N., Chakraborty, B., Rout, C.S., 2019. VSe2-reduced graphene oxide as efficient cathode material for field emission. J. Phys. Chem. Solids 128, 384–390.

Ren, X., Pang, L., Zhang, Y., Ren, X., Fan, H., Liu, S.F., 2015. One-step hydrothermal synthesis of monolayer MoS 2 quantum dots for highly efficient electrocatalytic hydrogen evolution. J. Mater. Chem. A 3, 10693–10697.

Sakthivel, M., Sukanya, R., Chen, S.-M., Dinesh, B., 2018. Synthesis of two-dimensional Sr-Doped MoSe2 nanosheets and their application for efficient electrochemical reduction of metronidazole. J. Phys. Chem. C 122, 12474–12484.

Shi, Y., Zhou, Y., Yang, D.-R., Xu, W.-X., Wang, C., Wang, F.-B., Xu, J.-J., Xia, X.-H., Chen, H.-Y., 2017. Energy level engineering of MoS2 by transition-metal doping for accelerating hydrogen evolution reaction. J. Am. Chem. Soc. 139, 15479–15485.

Sundaresan, R., Mariyappan, V., Chen, S.-M., Ramachandran, B., Paulsamy, R., Rasu, R., 2023. Construction of an electrochemical sensor towards environmental hazardous 4-nitrophenol based on Nd (OH) 3-embedded VSe2 nanocomposite. Environ. Sci. Pollut. Res., 1–14

Tang, H., Dou, K., Kaun, C.-C., Kuang, Q., Yang, S., 2014. MoSe 2 nanosheets and their graphene hybrids: synthesis, characterization and hydrogen evolution reaction studies. J. Mater. Chem. a 2, 360–364.

Tang, W., Jian, J., Chen, G., Bian, W., Yu, J., Wang, H., Zhou, M., Ding, D., Luo, H., 2021. Carbon nanotube supported amorphous MoS2 via microwave heating synthesis for enhanced performance of hydrogen evolution reaction. Energy Mater Adv., 2021

Tanjila, N., Ahsan, M., Ben Aoun, S., et al, 2021. An Electrochemical Approach to As (V) Determination via an Interaction with Alizarin Red S in Aqueous Medium. Journal of Analytical Chemistry 76, 1449–1454.

Tilak, B.V., Rader, C.G., Conway, B.E., 1977. Overpotential decay behavior—II. Generalized treatment for reaction pathways involving discharge, recombination and electrochemical desorption of adsorbed intermediates. Electrochim. Acta 22, 1167–1178.

Ulusoy Ghobadi, T.G., Patil, B., Karadas, F., Okyay, A.K., Yilmaz, E., 2017. Catalytic properties of vanadium diselenide: a comprehensive study on its electrocatalytic performance in alkaline, neutral, and acidic media. ACS Omega 2, 8319–8329.

Wang, X., Gong, Y., Shi, G., Chow, W.L., Keyshar, K., Ye, G., Vajtai, R., Lou, J., Liu, Z., Ringe, E., 2014. Chemical vapor deposition growth of crystalline monolayer MoSe2. ACS Nano 8, 5125–5131.

Wang, X., Chen, Y., Zheng, B., Qi, F., He, J., Li, P., Zhang, W., 2016b. Few-layered WSe2 nanoflowers anchored on graphene nanosheets: a highly efficient and stable electrocatalyst for hydrogen evolution. Electrochim. Acta 222, 1293–1299.

Wang, X.-D., Xu, Y.-F., Rao, H.-S., Xu, W.-J., Chen, H.-Y., Zhang, W.-X., Kuang, D.-B., Su, C.-Y., 2016a. Novel porous molybdenum tungsten phosphide hybrid nanosheets on carbon cloth for efficient hydrogen evolution. Energy Environ. Sci. 9, 1468–1475.

Wu, P., Sun, G., Chen, Y., Xu, W., Zheng, H., Xu, J., Wang, L., Peng, D.-L., 2020. MoSe 2-Ni 3 Se 4 Hybrid Nanoelectrocatalysts and Their Enhanced Electrocatalytic Activity for Hydrogen Evolution Reaction. Nanoscale Res. Lett. 15, 1–10.

Xu, X., Zhao, H., Wang, R., Zhang, Z., Dong, X., Pan, J., Hu, J., Zeng, H., 2018. Identification of few-layer ReS2 as photo-electro integrated catalyst for hydrogen evolution. Nano Energy 48, 337–344.

Yan, M., Pan, X., Wang, P., Chen, F., He, L., Jiang, G., Wang, J., Liu, J.Z., Xu, X., Liao, X., 2017. Field-effect tuned adsorption dynamics of VSe2 nanosheets for enhanced hydrogen evolution reaction. Nano Lett. 17, 4109–4115.

Yang, M., Cheng, X., Li, Y., Ren, Y., Liu, M., Qi, Z., 2017. Anharmonicity of monolayer MoS2, MoSe2, and WSe2: A Raman study under high pressure and elevated temperature. Appl. Phys. Lett. 110, 93108.

Yang, H., Yang, T., Zhu, H., Zhang, M., Du, M., 2016a. Synthesis of MoSe2/carbon nanofibers hybrid and its hydrogen evolution reaction performance. Chem. Lett. 45, 69–71.

Yang, J., Zhang, F., Wang, X., He, D., Wu, G., Yang, Q., Hong, X., Wu, Y., Li, Y., 2016b. Porous molybdenum phosphide nano-octahedrons derived from confined phosphorization in UIO-66 for efficient hydrogen evolution. Angew. Chemie 128, 13046–13050.

Yi, Y., Du, X., Zhao, Z., Liu, Y., Guan, H., Liu, X., Pei, X., Zhang, S., Li, D., 2022. Coupling of metallic VSe2 and conductive polypyrrole for boosted sodium-ion storage by reinforced conductivity within and outside. ACS Nano 16, 7772–7782.

Zhang, Q., Chen, P., Chen, L., Wu, M., Dai, X., Xing, P., Lin, H., Zhao, L., He, Y., 2020b. Facile fabrication of novel Ag2S/Kg-C3N4 composite and its enhanced performance in photocatalytic H2 evolution. J. Colloid Interface Sci. 568, 117–129.

Zhang, J., Kang, W., Jiang, M., You, Y., Cao, Y., Ng, T.-W., Denis, Y.W., Lee, C.-S., Xu, J., 2017. Conversion of 1T-MoSe 2 to 2H-MoS 2x Se 2–2x mesoporous nanospheres for superior sodium storage performance. Nanoscale 9, 1484–1490.

Zhang, K., Li, C., Zhao, Y., Yu, X., Chen, Y., 2015a. Porous one-dimensional Mo 2 C–amorphous carbon composites: high-efficient and durable electrocatalysts for hydrogen generation. Phys. Chem. Chem. Phys. 17, 16609–16614.

Zhang, Y., Shi, J., Han, G., Li, M., Ji, Q., Ma, D., Zhang, Y., Li, C., Lang, X., Zhang, Y., 2015b. Chemical vapor deposition of monolayer WS2 nanosheets on Au foils toward direct application in hydrogen evolution. Nano Res. 8, 2881–2890.

Zhang, S., Wang, G., Jin, J., Zhang, L., Wen, Z., Yang, J., 2018. Robust and conductive red MoSe2 for stable and fast lithium storage. ACS Nano 12, 4010–4018.

Zhang, L., Zhu, J., Wang, Z., Zhang, W., 2020a. 2D MoSe2/CoP intercalated nanosheets for efficient electrocatalytic hydrogen production. Int. J. Hydrogen Energy 45, 19246–19256.

Zhu, W., Tang, C., Liu, D., Wang, J., Asiri, A.M., Sun, X., 2016. A self-standing nanoporous MoP 2 nanosheet array: an advanced pH-universal catalytic electrode for the hydrogen evolution reaction. J. Mater. Chem. A 4, 7169–7173.

Zimron, O., Zilberman, T., Kadam, S.R., Ghosh, S., Kolatker, S., Neyman, A., Bar-Ziv, R., Bar-Sadan, M., 2020. Co-Doped MoSe2 nanoflowers as efficient catalysts for electrochemical hydrogen evolution reaction (HER) in acidic and alkaline media. Isr. J. Chem. 60, 624–629.